Self-Organized Bioelectricity via Collective Pump Alignment: Physical Origin of Chemiosmosis

Ryosuke Nishide◎* and Kunihiko Kaneko◎

Niels Bohr Institute, University of Copenhagen, Jagtvej 155 A, Copenhagen N, 2200, Denmark

Chemiosmosis maintains life in nonequilibrium through ion transport across membranes, yet the origin of this order remains unclear. We develop a minimal model in which ion pump orientation and the intracellular electrochemical potential mutually reinforce each other. This model shows that fluctuations can induce collective pump alignment and the formation of a membrane potential. The alignment undergoes a phase transition from disordered to ordered, analogous to the Ising model. Our results provide a self-organizing mechanism for the emergence of bioelectricity, with implications for the origin of life.

Coupling between directional ion transport across a membrane and the generation of an electrochemical potential difference is essential for living cells[1]. Mitchell's chemiosmotic theory established that electric currents operate at the source of life: nonequilibrium ion currents across membranes drive cellular energy transduction, including ATP synthesis[2–4]. Through this coupling, living systems are maintained far from equilibrium by sustained directional ion fluxes across membranes.

At the origin of life, the emergence of sustained nonequilibrium ion flows across membranes is thought to have been a critical step. Phylogenetic evidence indicates that early life already synthesized ATP through membrane-potential–driven processes[5, 6], and chemical and geological studies suggest that early cells may have emerged by exploiting natural proton gradients associated with alkaline hydrothermal vents[7, 8]. However, cells can autonomously generate membrane potential through ion transport, even in the absence of pre-existing ion gradients, leaving the origin of such mechanisms unresolved. Therefore, to elucidate the origin of life or protocells, it is necessary to understand how ion pumps could collectively generate and sustain membrane potential.

Although studies on the origin of life have examined the necessity of autocatalytic reaction sets[9–12], the generation of bio-information[13–18], the role of lipid membranes[19–21], and required nonequilibrium conditions[22, 23], how nonequilibrium flows and membrane potential mutually sustain each other remains an open physical problem. Here, we introduce a minimal model describing how ion pumps act collectively by exploiting electrochemical potentials that are generated self-consistently. We show that nonequilibrium ion transport by pumps and the membrane potential emerge through a phase transition analogous to that of the Ising model. We further discuss the conditions for this transition, as well as the roles of fluctuations and symmetry-breaking fields.

In our model, protocells generate a membrane potential $\Delta\phi$ via the flow of ions Q into and out of the cell through membrane-embedded pumps $P =$
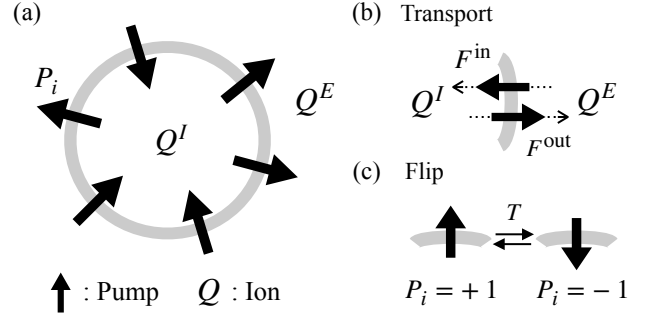

FIG. 1. Pump-ion coupling model, consisting of three regions; internal, external, and membrane. Pumps, $P = \{P_i\} = \{P_1, P_2, ..., P_{N_P}\}$, are embedded in a membrane and orient either inward ($P_i = +1$) or outward ($P_i = -1$). Ions are present in both the internal and external regions. Pumps and ions can interact with each other, resulting in 'flip' of pumps and 'transport' of ions. The direction of the arrows indicates the direction of ion transport; influx (F^{in}) and outflux (F^{out}).

$\{P_1, P_2, ..., P_{N_P}\}$, with the total number of pumps N_P fixed (Fig. 1). The total ion number N_Q is set to be constant and assumed to be sufficiently large for continuum approximation of concentrations $c^{I/E}$. Each pump is structurally asymmetric, and the direction of ion transport is determined by whether its head (ion-uptake side) faces inward or outward[24–26]. We represent the direction of the i-th pump by a binary variable $P_i \in \{-1, 1\}$, corresponding to inward and outward directions, respectively.

First, the ions are transported across the membrane by chemically driven pumps[35], in the presence of the electric potential barrier of the lipid bilayer[27–30]. The ion fluxes into and out of the cell are proportional to the number of inward and outward pumps, $n_P^{\text{in/out}}$, reflecting the structural asymmetry of the pumps. In addition, the ion flux depends on the electrochemical potential difference $\Delta\mu = \mu^I - \mu^E$ across the membrane, and, within a single Eyring-type barrier approximation[27–30], it is proportional to $\exp(\mu^{I/E})$. Here, $\mu^{I/E} = \mu_0 + \beta^{-1}\ln c^{I/E} + ze\phi^{I/E}$[31], where $\phi^{I/E}$ denotes the electrostatic potentials inside and outside the cell[36].

Summarizing the above, ion transport is expressed as follows[37]:

$$\partial_t c^I = \gamma n_P^{\text{in}} c^E \exp(\beta z e \phi^E) - \gamma n_P^{\text{out}} c^I \exp(\beta z e \phi^I), \quad (1)$$

where γ is the rate including chemical contributions to the pump[38]. Since N_P is fixed, $n_P^{\text{out}} = N_P - n_P$, where $n_P \equiv n_P^{\text{in}}$ hereafter. The external ion concentration, determined by ion-number conservation, is given by $c^E = r_V(c_0 - c^I) + c_0$, where $c_0 = N_Q/(V^I + V^E)$ is the average ion concentration and $r_V = V^I/V^E$ is the volume ratio. In addition, the membrane potential $\Delta\phi = \phi^I - \phi^E$ is expressed as

$$\Delta\phi = c_0 V^I \frac{ze}{C} q, \quad (2)$$

where C is the membrane capacitance, and we define the ion concentration ratio $q = (c^I - c_0)/c_0$[39]. Using the above definitions, the ion transport equation, Eq. (1), is given by

$$\partial_t q = \gamma(N_P - n_P)(1 - r_V q)e^{-\alpha q} - \gamma n_P(1 + q)e^{\alpha q}, \quad (3)$$

where $\alpha = \beta c_0 V^I z^2 e^2/(2C)$ quantifies the electrostatic energy associated with q, relative to thermal energy β^{-1} (see End Matter).

Next, we incorporate the interaction between the pumps and the membrane potential. The pumps are embedded in the membrane and equipped with a charged head, so that its orientation can change depending on the electrostatic potential, i.e., when the intracellular potential is low, the positively charged head tends to orient inward[40]. We introduce this effect by defining the energy associated with the interaction between the pump orientation and the electric field crossing the membrane as follows:

$$H(q, P) = z e J \Delta\phi \sum_i P_i, \quad (4)$$

where J denotes a coupling constant. Since $\Delta\phi$ depends on the ion concentration via Eq. (2), this gives an interaction between the pumps and the ions. The time evolution of the distribution of pump directions, $\pi(P, t)$, is determined by the following master equation with a single-pump flipping rate T:

$$\partial_t \pi(P, t) = \sum_l \{T(P|P^l)\pi(P^l, t) - T(P^l|P)\pi(P, t)\}, \quad (5)$$

$$T(P^l|P) = \exp\left[-\frac{\beta}{2}\{H(q, P^l) - H(q, P)\}\right], \quad (6)$$

where P^l denotes the configuration given by flipping the l-th pump in P. Recall that in the absence of a membrane potential, the energy Eq. (4) is zero. Then the pump direction fluctuates randomly between both directions around $n_P = N_P/2$. Consequently, according to Eq. (3), $q = 0$ follows, and there is no net directional ion
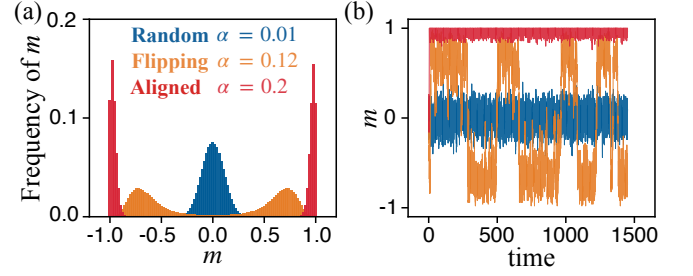

FIG. 2. Distribution for three states of pumps for 2000 samples (a) and their time series for one sample (b). Colors correspond to states: random (blue, $\alpha = 0.01$), flipping (yellow, $\alpha = 0.12$), and aligned (red, $\alpha = 0.2$). Parameters $N_P = 100, J = 5.5, \gamma = 1$. Frequency in (a) is calculated over $t = 30$–70 and normalized so that the total amount is one.

transport, so that the membrane potential disappears. Note that the transition probability in Eq. (5) with the energy (4) has the same form as the interaction between spins and an external field in the Ising mode, but, as mentioned above, there is a key difference: the potential is generated by the pump-driven nonequilibrium ion transport.

The time evolution of the membrane potential (or ion abundances) and the pump direction is investigated using Eqs. (3) and (5). We use a hybrid simulation approach: the dynamics of the pump directions are calculated using the Gillespie algorithm, whereas the dynamics of the ion concentration are described using an ordinary differential equation. Note that Eq. (3) is not deterministic because the dynamics depend on the stochastic change of pump directions. See Supplemental Material[34] for detailed simulation methods.

We first examine the simple case $r_V = 1$ in Eq. (3), where q takes values $-1 \leq q \leq 1$ (i.e., from all ions outside to inside). We then investigate the time evolution of pump alignment by setting $N_P = 100$ and $\gamma = 1$ for different values of α. After simulation time $t = 10$, the system reaches a steady state, where three distinct states are observed; random, flipping, and aligned states. In Fig. 2, histograms (for 2000 samples) and time series (for one sample) of the pump alignment order parameter

$$m = \frac{1}{N_P} \sum_i P_i = 2p - 1, \quad (7)$$

are plotted, where $p = n_P/N_P$. For small α (say 0.01), no pump alignment is observed. The distribution of m exhibits a single peak with zero mean and fluctuations around it (Fig. 2(a)). As α increases (e.g., $\alpha = 0.12$), the pumps mostly align, while their orientations intermittently switch between opposite directions (Fig. 2(b)). The distribution of m is bimodal, with broad peaks around ± 0.7, reflecting this switching behavior (Fig. 2(a)). As α further increases (e.g., $\alpha = 0.2$), the pumps become fully aligned either inward or outward,

depending on the sample. The distribution of m exhibits sharp peaks close to ± 1[37], and the alignment direction remains fixed over time for a given sample (Fig. 2). Note that no ion concentration difference appears in the absence of pump alignment (SFig. 1[34]), whereas the collective pump alignment induces an ion concentration bias and a membrane potential. The distributions of pump alignment and ion concentration reflect the symmetry of the system under the transformation $(m, q) \to (-m, -q)$.

To characterize the transitions among these states, we plot the time-averaged ensemble mean of $|m|$[41], $\langle|m|\rangle$, and its variance $\langle\delta|m|^2\rangle$[42], against J and α. In Fig. 3(a), as α or J increases, the random state (blue region) transitions to the aligned state (red region). Figure 3(b) shows that the flipping rate is enhanced near the transition region. Additionally, the order parameter $\langle|m|\rangle$ increases sharply and its variance shows a sharp peak near $\alpha = 0.1$ at $J = 5.5$ (Figs. 3(c) and (d)). Hence, the change between the random and aligned states can be interpreted as a phase transition with the flipping state appearing as a critical phenomenon.

We now analyze the phase transition using the mean-field approach, motivated by the analogy between our model and the Ising model. In the random and aligned states, the steady-state ion concentration exhibits peaks at zero and ± 1, respectively, although $q(p)$ is affected by the fluctuation of pump orientations. We employ a mean-field approximation in which the fluctuation of p in $q(p)$ is neglected, $q(p) \simeq \bar{q}(\langle p \rangle) \equiv \bar{q}$. This corresponds to the electrostatic potential acting as a 'mean-field' for pumps. We then obtain a self-consistent equation for $\bar{q}$ (see End Matter):

$$\tanh(2J\alpha\bar{q}) = \tanh\left(\alpha\bar{q} + \tanh^{-1}\bar{q}\right). \tag{8}$$

The solution of this self-consistent equation exhibits a pitchfork bifurcation at critical α[34], given by

$$\alpha_C = \frac{1}{2}\frac{1}{J - \frac{1}{2}}. \tag{9}$$

For $\alpha < \alpha_C$, the self-consistent equation has a single stable solution at $\bar{q} = 0$, and accordingly $\langle\bar{m}\rangle = 0$, which corresponds to the random state. For $\alpha > \alpha_C$, there are three solutions: one unstable solution at $\bar{q} = 0$ and two stable solutions $\bar{q} = \pm q_s$, where q_s approaches one for $\alpha \gg \alpha_C$. The two stable solutions correspond to the aligned states. Hence, increasing α enhances the mutual reinforcement between the electric potential and pump alignment, inducing a transition from the entropy-dominant random phase to the aligned phase at $\alpha = \alpha_C$, with pump flipping appearing as a critical behavior. The mean-field critical line [Eq. (9)] agrees well with the numerical results (Fig. 3).

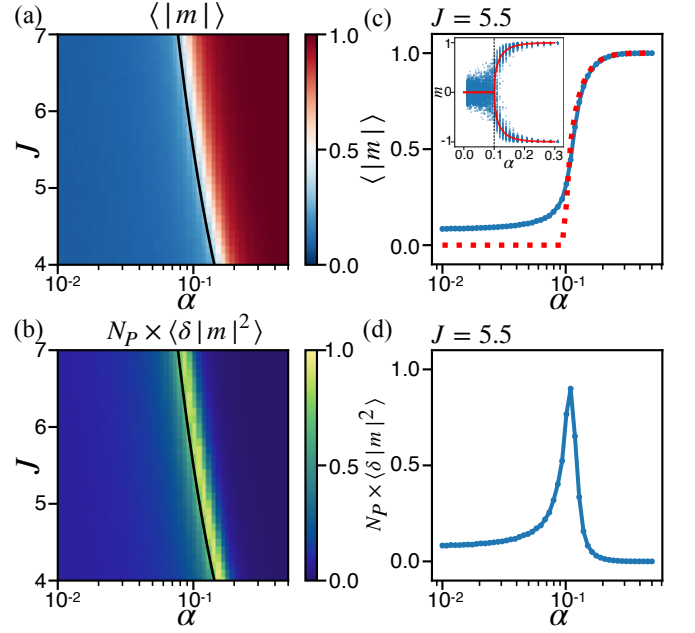Near $\alpha = \alpha_C$, expanding Eq. (8) around $\bar{q} = 0$ yields

FIG. 3. Phase diagram. (a) time-averaged ensemble mean of $|m|$ against J and α. (b) variance of $|m|$ multiplied by N_P plotted against J and α. (c) time-averaged ensemble mean of $|m|$ (blue), m at $t = 70$ (blue in inset), and stable solutions of self-consistent equation (8) (red), against α at $J = 5.5$. (d) variance of $|m|$ multiplied by N_P plotted against α at $J = 5.5$. (a),(b) transition lines $J = 1/(2\alpha) + 1/2$ (black). Parameters $N_P = 100, \gamma = 1$, and 200 samples. The mean and variance are calculated from the samples at each time, then the time-averaged values are taken over $t = 30$–70.

the following critical behavior (see End Matter):

$$\bar{q} \sim \pm\sqrt{3}\Delta\alpha^{\frac{1}{2}}, \tag{10}$$

$$\langle\bar{m}\rangle \sim \mp\sqrt{3}(1 + \alpha_C)\Delta\alpha^{\frac{1}{2}}, \tag{11}$$

where $\Delta\alpha = (\alpha - \alpha_C)/\alpha_C > 0$. These results exhibit the transition with the critical exponents $1/2$. The self-consistent solution is plotted as the red line in Fig. 3(c), which agrees well with numerical simulations, except for small deviation at low α due to large fluctuations around $\langle\bar{m}\rangle = 0$. Furthermore, as shown in SFig. 2[34], the slope of $\langle\bar{m}\rangle$ becomes steeper as N_P increases, and the transition point approaches that given by Eq. (9).

Unlike the mean-field Ising model, the critical behavior of $\langle\bar{m}\rangle$ depends on the coefficient $1+\alpha_C$. This dependence is negligible when α is small and J is large. Indeed, by fixing $J\alpha$ and taking the limit $\alpha \to 0$, Eq. (8) yields,

$$\tanh(J\alpha\langle\bar{m}\rangle) = \langle\bar{m}\rangle, \tag{12}$$

i.e., the self-consistent equation for the mean-field Ising model. In addition, Eq. (9) shows the absence of a phase transition for $J < 1/2$ (see also SFig. 3[34]). This reflects the fact that macroscopic pump alignment requires the energy gain from pump flipping to exceed the electrochemical potential cost of ion transport (see End Matter).

Moreover, our mean-field analysis effectively treats the system as if it were in equilibrium; however, it is intrinsically nonequilibrium with detailed balance broken[34]. Accounting for the nonequilibrium nature is necessary to reveal the critical behavior associated with the pump fluctuation, such as variances.

Finally, we investigate the effects of the volume difference r_V using Eq. (3), also by adding the term for backward reaction also included[43]. Is this case, there also exists a phase transition from the random state to the aligned state as α increases. Unlike the case $r_V = 1$, however, by increasing α from the random state, the pump-alignment state first appears only in the inward direction (Fig. 4). Upon further increase in α, aligned states in both directions appear. In addition, as r_V decreases, the transition line shifts toward smaller α, and the flipping state is suppressed. The effect of $r_V < 1$ is revealed by the self-consistent equation (see End Matter):

$$\tanh(2J\alpha\bar{q}) = \eta \tanh\left(\alpha\bar{q} + \frac{1}{2}\ln\frac{1+\bar{q}}{1-r_V\bar{q}}\right), \qquad (13)$$

where $\eta = (\gamma+\gamma^b)/(\gamma-\gamma^b) \simeq 1$. Fixing r_V and increasing α lead to stable fixed points at $\bar{q} = 0$ and $\bar{q} = q_+ > 0$, separated by an unstable fixed point $\bar{q} = q_- < 0$. For small α, fluctuations dominate and the system remains in the random phase ($\bar{q} = \langle \bar{m} \rangle = 0$). As α increases, alignment becomes favorable; in particular, the energy (4) becomes lower for the inward pump alignment than for the opposite direction, resulting in a symmetry-broken aligned state ($\bar{q} = q_+, \langle \bar{m} \rangle \simeq -1$). With further increase in α, $\bar{q} = 0$ becomes unstable and $\bar{q} = q_-$ becomes stable via a locally transcritical–like bifurcation, at

$$\alpha_C = \frac{1+r_V}{4}\frac{\eta}{J-\frac{\eta}{2}}, \qquad (14)$$

so that for $\alpha > \alpha_C$, both inward ($\bar{q} = q_+$) and outward ($\bar{q} = q_-$) aligned states are stable[44]. However, Fig. 4 shows pump alignment remains biased inward even slightly beyond the transition line. This occurs because, for α close to α_C, the fixed point $\bar{q} = q_-$ is close to zero, so fluctuations are strong and inward orientation is preferentially observed. For sufficiently large α, alignment in both directions is realized. Furthermore, decreasing r_V enhances the energy asymmetry and suppresses fluctuations around $\bar{q} = q_+$, thereby expanding the range of α over which inward orientation is observed and pump flipping is suppressed (Fig. 4).

Note that asymmetry between the two pump alignment directions also exists when the inward and outward transport rates differ[45], i.e., $r_\gamma = \gamma^{\text{in}}/\gamma^{\text{out}} \neq 1$. The parameter r_γ plays a role analogous to a symmetry-breaking field in the Ising model (see End Matter), causing the self-consistent equation to no longer pass through the origin, thereby inducing asymmetric alignment and hysteresis (SFig. 4[34])[46].
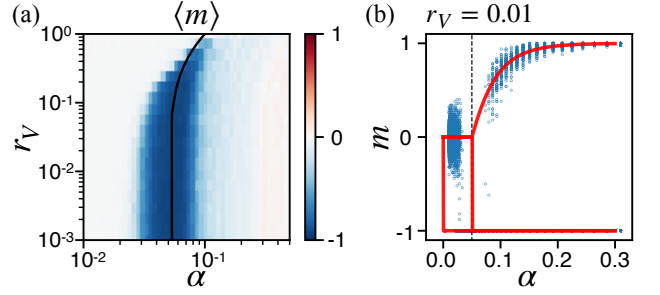

FIG. 4. r_V dependence of pumps alignment. (a) time-averaged ensemble mean of m against r_V and α. The black line shows bifurcation line $r_V = 2\alpha(2J/\eta - 1) - 1$ (see End Matter). (b) m at $t = 100$ for 200 samples (blue) and stable solutions of self-consistent equation (13) (red), against α at $r_V = 0.01$. Parameters $N_P = 100, \gamma = 1, J = 5.5$, and 200 samples. The mean is calculated from the samples at each time, then the time-averaged values are taken over $t = 0$–100.

In conclusion, we demonstrated that a membrane potential and directional ion transport are self-organized through the collective alignment of ion pumps, which enables chemiosmosis. As the pump-ion coupling (J) or the electrostatic coupling (α) increases, a phase transition occurs from zero to a finite membrane potential along with pump alignment. This transition and its critical behavior are explained by mean-field analysis. Although analogous to the mean-field Ising transition, the system is intrinsically out of equilibrium. Additionally, volume or transport asymmetries act as symmetry-breaking fields, biasing pump orientation.

Our results provide new insights into the origin of life. Nick Lane et al. proposed that protocells could use externally-supplied ion gradients to evolve into life[7]. While this was one plausible pathway, our results suggest an alternative: membrane potential and directional ion transport arise spontaneously via simple ion–pump interactions, producing self-organized bioelectricity without pre-existing gradients. Such a gradient could then act as an auxiliary symmetry-breaking field, in addition to the asymmetry in volume or transport ratio demonstrated here. Moreover, fluctuations give rise to self-organized pump alignment, indicating that early systems likely had a moderate number of pumps, as larger numbers would slow alignment. Finally, changes in the molecular composition of the membrane or pumps could alter J and α, allowing them to exceed a critical point and, leading to the emergence of bioelectricity.

Extending this model to multiple ion species and explicit pump kinetics[26–28] will further clarify the emergence of membrane potentials. In particular, although γ is assumed constant at present, it can in reality depend on pump-driving chemical reactions that are themselves facilitated by pump activity. Incorporating this feedback may change $\gamma^{\text{in/out}}$, enhancing asymmetry in pump orientation and stabilizing directional ion trans-

port. Finally, our model poses an interesting problem in statistical physics, as it is intrinsically out of equilibrium unlike the traditional Ising model.

ACKNOWLEDGEMENT

---

* ryosuke.nishide@nbi.ku.dk

[1] B. Schoepp-Cothenet, R. van Lis, A, Atteia, F. Baymann, L. Capowiez, A.-L. Ducluzeau, S. Duval, F. ten Brink, M. J. Russell, and W. Nitschke, On the universal core of bioenergetics, Biophysica Acta (BBA)-Bioenergetics, **2**, 79–93 (2013).

[2] P. Mitchell, Coupling of phosphorylation to electron and hydrogen transfer by a chemi-osmotic type of mechanism, Nature, **191**, 144–148 (1961).

[3] P. Mitchell, Chemiosmotic coupling in oxidative and photosynthetic phosphorylation, Biological Reviews, **41**, 445–501 (1966).

[4] A. M. Morelli, S. Ravera, D. Calzia, and I. Panfoli, An update of the chemiosmotic theory as suggested by possible proton currents inside the coupling membrane, **9**, 180221 (2019).

[5] M. C. Weiss, F. L. Sousa, N. Mrnjavac, S. Neukirchen, M. Roettger, S. Nelson-Sathi, and W. F. Martin, The physiology and habitat of the last universal common ancestor, Nature microbiology, **1**, 1–8 (2016).

[6] E. R. R. Moody, S. Álvarez-Carretero, T. A. Mahendrarajah, J. W. Clark, H. C. Betts, N. Dombrowski, L. L. Szánthó, R. A. Boyle, S. Daines, X. Chen, N. Lane, Z. Yang, G. A. Shields, G. J. Szöllősi, A. Spang, D. Pisani, T. A. Williams, T. M. Lenton, and P. C. J. Donoghue, The nature of the last universal common ancestor and its impact on the early Earth system, Nature Ecology & Evolution, **8**, 1654–1666 (2024).

[7] V. Sojo, A. Pomiankowsli, and N. Lane, A bioenergetic basis for membrane divergence in archaea and bacteria, PLoS biology, **12**, e1001926 (2014).

[8] F. Yu, J. Fei, Y. Jia, T. Wang, W. F. Martin, and J. Li, Chemiosmotic ATP synthesis by minimal protocells, Cell Reports Physical Science, **6** (2025).

[9] F. Dyson, Origins of life, Cambridge University Press (1999).

[10] S. Jain, and S. Krishna, A model for the emergence of cooperation, interdependence, and structure in evolving networks, Proceedings of the National Academy of Sciences, **98**, 543–547 (2001).

[11] A. Blokhuis, D. Lacoste, and P. Nghe, Universal motifs and the diversity of autocatalytic systems, Proceedings of the National Academy of Sciences, **117**, 25230–25236 (2020).

[12] K. Kaneko, On recursive production and evolvability of cells: catalytic reaction network approach, Geometric Structures of Phase Space in Multidimensional Chaos: Applications to Chemical Reaction Dynamics in Complex Systems, **130**, 543–598 (2005).

[13] S. A. Kauffman, The origins of order: Self-organization and selection in evolution, In Spin glasses and biology, 61–100 (1992).

[14] M. Eigen, Selforganization of matter and the evolution of biological macromolecules, Naturwissenschaften, **58**, 465–523 (1971).

[15] M. Eigen and P. Schuster, The hypercycle: a principle of natural self-organization, Springer Science & Business Media (2012).

[16] K. Kaneko and T. Yomo, On a kinetic origin of heredity: minority control in a replicating system with mutually catalytic molecules, Journal of theoretical biology, **214**, 563–576 (2002).

[17] A. V. Tkachenko and S. Maslov, Spontaneous emergence of autocatalytic information-coding polymers, The Journal of Chemical Physics, **143** (2015).

[18] M. J. Falk, L. Zhou, Y. J. Matsubara, K. Husain, J. W. Szostak, and A. Murugan, Suppression of errors in collectively coded information, arXiv:2508.21806.

[19] D. Segré, D. Ben-Eli, D.W. Deamer, and D. Lancet, The lipid world, Origins of Life and Evolution of the Biosphere, **31**, 119–145 (2001).

[20] D. Lancet, R. Zidovetzki, and O. Markovitch, Systems protobiology: origin of life in lipid catalytic networks, Journal of The Royal Society Interface **15**, 20180159 (2018).

[21] E. Szathmáry, The origin of replicators and reproducers, Philosophical Transactions of the Royal Society B: Biological Sciences, **361**, 1761–1776 (2006).

[22] N. Goldenfeld and C. Woese, Life is physics: evolution as a collective phenomenon far from equilibrium, Annu. Rev. Condens. Matter Phys., **2**, 375-399 (2011).

[23] E. Branscomb, T. Biancalani, N. Goldenfeld, and M. Russell, Escapement mechanisms and the conversion of disequilibria; the engines of creation, Phys. Rep. **677**, 1–60 (2017).

[24] J. P. Morth, B. P. Pedersen, M. J. Buch-Pedersen, J. P. Andersen, B. Vilsen, M. G. Palmgren, and P. Nissen, A structural overview of the plasma membrane Na+, K+-ATPase and H+-ATPase ion pumps, Nature reviews Molecular cell biology **12**, 60–70 (2011).

[25] M. Dyla, M. Kjærgaard, H. Poulsen, and P. Nissen, P, Structure and mechanism of P-type ATPase ion pumps. Annual review of biochemistry, **89**, 583-603 (2020)

[26] F. Calisto, F. M. Sousa, F. V. Sena, P. N. Refojo, and M. M. Pereira, Mechanisms of energy transduction by charge translocating membrane proteins, Chemical reviews, **121**, 1804–1844 (2021).

[27] D. A. Beard, A biophysical model of the mitochondrial respiratory system and oxidative phosphorylation, PLoS computational biology **1**, e36 (2005).

[28] G. Terradot, E. Krasnopeeva, P. S. Swain, and T. Pilizota, Escherichia coli Maintains pH via the Membrane Potential, Physical Review X, **2**, 043015 (2024).

[29] W. Lo, E. Krasnopeeva, and T. Pilizota, Bacterial electrophysiology, Annual Review of Biophysics, **53** (2024).

[30] K. D. Garlid, A. D. Beavis, and S. K. Ratkje, On the nature of ion leaks in energy-transducing membranes, Biochimica et Biophysica Acta (BBA)-Bioenergetics, **12**, 109–120 (1989).

[31] D. Kondepudi and I. Prigogine, Modern thermodynamics: from heat engines to dissipative structures, John wi-

ley & sons (2014).

[32] G. Von Heijne, Membrane-protein topology, Nature reviews Molecular cell biology, **7**, 909–918 (2006).

[33] M. Bogdanov, H. Vitrac, and W. Dowhan, Flip-flopping membrane proteins: how the charge balance rule governs dynamic membrane protein topology, Biogenesis of Fatty Acids, Lipids and Membranes, 1–28 (2018).

[34] See Supplemental Material for details of simulation method, calculation, and supplemental figures.

[35] Ions are passively transported via membrane-embedded ion channels and leakage. For simplicity, we assume that ion transport is dominated by pumps, and neglect ion channels and leakage. While channels and leakage act to reduce ion concentration gradients, they do not qualitatively affect our results.

[36] The reference chemical potential μ_0 is common to both regions and can be absorbed into the kinetic prefactor. β, z, and e are inverse temperature, the valence of ion, and the elementary charge, respectively.

[37] For simplicity, here we neglect the backward reaction.

[38] For simplicity, we set γ to be constant.

[39] $q = 0$ corresponds to $c^I = c^E = c_0$, indicating the absence of a membrane potential.

[40] The orientation of membrane proteins is characterized by the positive-inside rule[32], whereby residues with positive charge face the cytoplasmic side, reflecting differences in charge and electrostatic potential across the membrane. The orientation can reverse in response to alterations in the charge distribution of residues[33].

[41] Since the pumps align bidirectionally, the state is characterized by the absolute value of m.

[42] $\delta|m| = |m| - \langle|m|\rangle$.

[43] For small r_V, q can take large values ($-1 \le q \le 1/r_V$), so that the backward reaction becomes non-negligible. Here we use a backward pumping rate, $\gamma^b = 10^{-5}$.

[44] Eq. (14) represents a generalization of Eq. (9).

[45] This occurs when the chemical reactions driving the pumps are asymmetric between the interior and exterior.

[46] r_γ represents the ratio of the pumping strength of the interior to that of the exterior, where $r_\gamma \ne 1$ leads to a steady state $\bar{q} \ne 0$. This results in a shift from the origin with a contribution of $(\ln r_\gamma)/2$, as in Eq. (40). In contrast, the term with r_V, even for $r_V \ne 1$, always keeps a steady-state solution $\bar{q} = 0$, which induces concentration-dependent deviation, as in Eq. (36).

[47] Note that we here consider the large N_P limit, treat p as a continuous variable, and use the mean-field value of q.

END MATTER

Membrane potential

The membrane potential $\Delta\phi$ arises from an imbalance of charges across the membrane, which has low ion permeability and acts as a capacitor[29]. It is defined as the difference between the net charges inside, $\mathcal{Q}^I_{\text{net}}$, and outside, $\mathcal{Q}^E_{\text{net}}$, the cell:

$$\Delta\phi = \frac{1}{C}(\mathcal{Q}^I_{\text{net}} - \mathcal{Q}^E_{\text{net}}) = \frac{e}{C}\sum_i (z_i n_i^I - z_i n_i^E), \quad (15)$$

where $n_i^{I/E}$ is the numbers of internal/external ions of type i, z_i is the valence of ions i, and C is the membrane capacitance. Assuming only ions Q can transport across the membrane and other ions have no gradient,

$$c_j \equiv \frac{n_j^I}{V^I} = \frac{n_j^E}{V^E}, \quad \forall j \ne Q, \quad (16)$$

the net charges satisfy $\mathcal{Q}^I_{\text{net}} = -\mathcal{Q}^E_{\text{net}}$. With the total number $N_Q = n_Q^I + n_Q^E$, the membrane potential can be expressed as

$$\Delta\phi = \frac{z_Q e}{C}\left(n_Q^I - \frac{V^I N_Q}{V^I + V^E}\right) = \frac{z_Q e V^I}{C}(c^I - c_0), \quad (17)$$

where $c^I = n_Q^I/V^I$ is the internal concentration of Q and $c_0 = N_Q/(V^I + V^E)$ is the average concentration. Internal and external potentials relative to the membrane surface are then

$$\phi^I = -\phi^E = \frac{\Delta\phi}{2}. \quad (18)$$

Mean-field analysis and self-consistent equation

We derive the self-consistent equation (8) using a mean-field analysis. In the steady state, we define $\pi^*(p)$ as the steady distribution of p, and $q^*(p)$ as the steady solution of Eq. (3). In the large N_P, the distribution $\pi^*(p)$ becomes sharply peaked around its mean value $\langle p \rangle = \sum p\pi^*(p)$, leading to $p = \langle p \rangle + \delta p$, where $|\delta p|$ is sufficiently small. As a consequence, the stationary solution can be approximated as $q^*(p) \simeq q^*(\langle p \rangle) \equiv \bar{q}$, and fluctuations associated with δp are neglected to leading order. Within the approximation, the energy (4) is evaluated using $\bar{q}$ as the mean field,

$$\bar{H}(P) = \frac{2J\alpha\bar{q}}{\beta}\sum_i P_i, \quad (19)$$

where, i.e., the electric potential $\alpha\bar{q}$ corresponds to the mean field. Then, the detailed balance is satisfied, and the steady distribution is approximated by the Boltzmann distribution, denoted by $\bar{\pi}^*(p)$. For convenience,

we introduce the distribution with respect to P, denoted by $\bar{\pi}^*(P)$, which is given by

$$\bar{\pi}^*(P) = \frac{e^{-\beta\bar{H}(P)}}{Z}, \ Z = \cosh^{N_P}(2J\alpha\bar{q}). \quad (20)$$

The statistical mean of m is then given by

$$2\langle\bar{p}\rangle - 1 = -\frac{1}{2J\alpha}\frac{\partial\ln Z}{\partial\bar{q}} = -\tanh(2J\alpha\bar{q}) \equiv \langle\bar{m}\rangle, \quad (21)$$

where we use $\langle\bar{p}\rangle \equiv \sum p\bar{\pi}^*(p)$. Next, taking the average of Eq. (3) under $r_V = 1$ with respect to the $\bar{\pi}^*(p)$ and using the approximation $q^*(p) \simeq \bar{q}$, we obtain the steady-state condition $\partial_t\bar{q} = 0$ as

$$\langle\bar{p}\rangle = \frac{1 - \bar{q}}{(1 + \bar{q})e^{2\alpha\bar{q}} + 1 - \bar{q}}. \quad (22)$$

Using Eqs. (7), (21), and (22), we obtain the self-consistent equation for $\bar{q}$:

$$\tanh(2J\alpha\bar{q}) = \frac{(1 + \bar{q})e^{2\alpha\bar{q}} - (1 - \bar{q})}{(1 + \bar{q})e^{2\alpha\bar{q}} + (1 - \bar{q})}. \quad (23)$$

Using the sum formula of hyperbolic tangent, we get Eq. (8). Since $\tanh(\cdot)$ is a monotonic function, which yields

$$\bar{q} = \tanh((2J - 1)\alpha\bar{q}). \quad (24)$$

Thus, the bifurcation line is given by

$$(2J - 1)\alpha = 1. \quad (25)$$

Hence, for $(2J - 1)\alpha < 1$, there is one stable solution, $\bar{q} = 0$, whereas for $(2J - 1)\alpha > 1$, there are two stable solutions, $\bar{q} = \pm q_s$, and one unstable solution, $\bar{q} = 0$.

Critical exponent

In the vicinity of $\bar{q} = 0$, we expand the left-hand side and right-hand side of self-consistent equation (8) as

$$\text{LHS} = \frac{1 + \alpha_C}{\alpha_C}\bar{q} - \frac{1}{3}\left(\frac{1 + \alpha_C}{\alpha_C}\right)^3\alpha^3\bar{q}^3 + \mathcal{O}(\bar{q}^5), \quad (26)$$

$$\text{RHS} = (1 + \alpha)\bar{q} - \left(\alpha + \alpha^2 + \frac{1}{3}\alpha^3\right)\bar{q}^3 + \mathcal{O}(\bar{q}^5), \quad (27)$$

where we used $J = 1/(2\alpha_C) + 1/2$. Up to third order, the nonzero solutions are given by

$$\bar{q}^2 \simeq \frac{\alpha - \alpha_C}{\alpha_C}\left\{\left(\frac{1}{3\alpha_C^3} + \frac{1}{\alpha_C^2} + \frac{1}{\alpha_C}\right)\alpha^3 - \alpha^2 - \alpha\right\}^{-1}. \quad (28)$$

Thus, for small $\Delta\alpha = (\alpha - \alpha_C)/\alpha_C > 0$, retaining only the leading-order contribution yields Eqs. (10) and (11).

Bound of J for the transition

From Eq. (9), the alignment phase does not appear for $J < 1/2$. This can be understood in terms of the competition between ion transport and pump flipping in the random phase. We describe the ion transport using the effective chemical potentials $\mu^{I/E}$ and the effective work terms $w^{I/E}$, as

$$\partial_t q = e^{\mu^E + w^E} - e^{\mu^I + w^I}, \quad (29)$$

where, for simplicity, we set $\beta = 1$ and $\bar{\gamma} = \gamma N_P$, and

$$\begin{cases} \mu^E = \ln(1 - q) - \alpha q, & w^E = \ln\{\bar{\gamma}(1 - p)\}, \\ \mu^I = \ln(1 + q) + \alpha q, & w^I = \ln(\bar{\gamma}p). \end{cases} \quad (30)$$

The total chemical potential associated with the ion transport into the cell is

$$\mu_{\text{ion}} = \mu^I + w^I - (\mu^E + w^E)$$
$$= \ln\frac{1 + q}{1 - q} + 2\alpha q + \ln\frac{p}{1 - p}. \quad (31)$$

For pump flipping, the chemical potential is

$$\mu_{\text{flip}} = \ln\frac{1 - p}{p} + 4J\alpha q, \quad (32)$$

where a positive μ_{flip} favors a flip that decreases p, and vice versa[47]. At the phase transition, the solution $(q, p) = (0, 1/2)$ needs to be unstable, and is replaced by the aligned state. To see the condition for this to occur, consider a microstate in which the ion concentration has increased by an infinitesimal amount $dq > 0$, i.e., $(q, p) = (dq, 1/2)$. At this state, there are two competing processes: (i) an inward pump flip, and (ii) a return of the ions, which would bring q back to zero. The chemical potential decrease associated with an inward pump flip is $d\mu_{\text{flip}}^\star = 4J\alpha dq$. In contrast, the chemical potential decrease associated with returning the ions is $d\mu_{\text{ion}}^\star = (2 + 2\alpha)dq$. Comparing the magnitudes of these chemical potentials, the macroscopic alignment phase occurs only if the pump flip is favored over ion return, i.e.,

$$d\mu_{\text{flip}}^\star > d\mu_{\text{ion}}^\star \quad \Rightarrow \quad J \geq \frac{1}{2} + \frac{1}{2\alpha}. \quad (33)$$

As $\alpha > 0$, the lower bound reduces to $J = 1/2$.

Result for r_V

The ion concentration dynamics obtained by adding the backward reaction to Eq. (3) is given by

$$\partial_t q = \gamma(N_P - n_P)(1 - r_V q)e^{-\alpha q} - \gamma n_P(1 + q)e^{\alpha q}$$
$$- \gamma^b(N_P - n_P)(1 + q)e^{\alpha q} + \gamma^b n_P(1 - r_V q)e^{-\alpha q}. \quad (34)$$

Using the mean-field approximation, we obtain the self-consistent equation:

$$\tanh(2J\alpha\bar{q}) = \eta \tanh\left(\alpha\bar{q} + \frac{1}{2}\ln\frac{1 - r_V\bar{q}}{1 - \bar{q}}\right). \qquad (35)$$

Since $\eta = (\gamma + \gamma^b)/(\gamma - \gamma^b) = 1 + \mathcal{O}\{(\gamma^b/\gamma)^2\} \simeq 1$ and $\tanh(\cdot)$ is a monotonic function, we obtain

$$\bar{q} \simeq \tanh\left((2J - 1)\alpha\bar{q} + \frac{1}{2}\ln\frac{1 - r_V\bar{q}}{1 - \bar{q}}\right). \qquad (36)$$

This consistent with the self-consistent equation of mean-field Ising model under the external field depending on $\bar{q}$. The derivative of the left-hand side minus the right-hand side of self-consistent equation at $\bar{q} = 0$ shows that the stability of the $\bar{q} = 0$ state changes across the following line:

$$\alpha = \frac{1 + r_V}{4}\frac{\eta}{J - \frac{\eta}{2}}. \qquad (37)$$

Result for r_γ

When the inward and outward transport rates differ, the ion concentration dynamics is given by

$$\partial_t q = \gamma^{\mathrm{in}}(N_P - n_P)(1 - q)e^{-\alpha q} - \gamma^{\mathrm{out}}n_P(1 + q)e^{\alpha q}. \qquad (38)$$

Using the mean-field approximation, obtain the self-consistent equation:

$$\tanh(2J\alpha\bar{q}) = \tanh\left(\tanh^{-1}\bar{q} + \alpha\bar{q} - \frac{1}{2}\ln r_\gamma\right). \qquad (39)$$

Since $\tanh(\cdot)$ is a monotonic function, which yields

$$\bar{q} = \tanh\left((2J - 1)\alpha\bar{q} + \frac{1}{2}\ln r_\gamma\right). \qquad (40)$$

This consistent with the self-consistent equation of mean-field Ising model under the external field $(\ln r_\gamma)/2$.